Journal of Hydraulic Research

ISSN: 0022-1686 (Print) 1814-2079 (Online) Journal homepage: https://www.tandfonline.com/loi/tjhr20

Benthic and interfacial mixing in a strongly-stratified estuary

M. Arthur Simanjuntak , Jörg Imberger , Keisuke Nakayama & Tadaharu Ishikawa

To cite this article: M. Arthur Simanjuntak , Jörg Imberger , Keisuke Nakayama & Tadaharu Ishikawa (2011) Benthic and interfacial mixing in a strongly-stratified estuary, Journal of Hydraulic Research, 49:6, 791-798, DOI: 10.1080/00221686.2011.607304

To link to this article: https://doi.org/10.1080/00221686.2011.607304

Published online: 14 Oct 2011.

Journal of Hydraulic Research Vol. 49, No. 6 (2011), pp. 791–798
http://dx.doi.org/10.1080/00221686.2011.607304

Research paper

Benthic and interfacial mixing in a strongly-stratified estuary

M. ARTHUR SIMANJUNTAK, PhD Candidate, *Centre for Water Research, University of Western Australia, Crawley, 6009, WA, Australia.*
Email: a.simanjuntak@bom.gov.au

JÖRG IMBERGER, Professor, *Centre for Water Research, University of Western Australia, Crawley, 6009, WA, Australia.*
Email: jimberger@cwr.uwa.edu.au (author for correspondence)

KEISUKE NAKAYAMA, Professor, *Department of Civil Engineering, Kitami Institute of Technology, Kohen-cho 165, Kitami City, Japan.*
Email: nakayama@mail.kitami-it.ac.jp

TADAHARU ISHIKAWA, Professor, *Department of Environmental Science and Technology, Interdisciplinary Graduate School of Science and Engineering, Tokyo Institute of Technology and Engineering, Nagatsuda Town, Midori-ku, Yokohama City 2268502, Japan.*
Email: ishikawa.t.ai@m.titech.ac.jp

ABSTRACT
Tone River is a shallow, tidal estuary with a controllable upstream freshwater discharge via a barrage. The mixing characteristics in the benthic and interfacial regions of the Tone River estuary were investigated during a time window of maximum freshwater discharge and high shear, using temperature and velocity microstructure measurements. Although the production of turbulent kinetic energy from mean shear was high throughout the water column, the intermittency of both up- and down-gradient buoyancy fluxes resulted in negligible net down-gradient mixing. These opposing fluxes were incorporated into a turbulent closure scheme by using the concept of percentage down-gradient flux. A comparison of vertical diffusivity from two alternative closures suggests that the stratification imposed a length scale limitation on the vertical turbulent excursions that proved crucial for the transition region between the benthic and interfacial regions; it is argued that a Richardson-number based closure is both conceptually and practically adequate to represent the effect of length-scale limitation and percentage down-gradient flux.

Keywords: Down-gradient flux, estuary, Richardson number, shear, turbulent closure

1 Introduction

The Tone River is the second longest river in Japan, flowing into the Pacific Ocean near Tokyo. An estuary barrage, located 18.5 km upstream of the river mouth, controls the river freshwater discharge. The barrage discharges freshwater during ebb tides and prevents salt water from intruding during rising tides. Ishikawa *et al.* (2004) showed that a persistent salt wedge forms downstream of the barrage, the water in which often becomes deoxygenated (hypoxic) and this low oxygen salt wedge water is subsequently transported downstream along the halocline, highlighting the importance of vertical mixing (Pawlak and Armi 1997, Coates *et al.* 2002). Direct turbulence measurements were carried out to investigate the mixing at the benthic and interfacial regions of the salt wedge during a period of high freshwater discharge and falling tide when the interfacial shear was large. Past studies suggest that the turbulent kinetic energy (TKE) generated by the build-up of shear across the pycnocline and enhanced by bottom friction generated stirring TKE, during late ebb, may lead to large scale mixing (Geyer and Smith 1987, Geyer and Farmer 1989, Grigg and Ivey 1997). Coates *et al.* (2002) showed that the mixing intensity, due to shear-induced billowing, decreases rapidly after the early stage of a "mixing" event, hence the time window of intense mixing was likely to be short lived and the mixing may be expected to be intermittent and patchy (Geyer and Smith 1987, Geyer and Farmer 1989, Jay and Smith 1990, Monismith and Fong 1996, Cudaback and Jay 2000).

Intermittent mixing in a strongly stratified water column involves counter-gradient vertical buoyancy fluxes (Gargett and

Revision received 12 July 2011/Open for discussion until 30 June 2012.

ISSN 0022-1686 print/ISSN 1814-2079 online
http://www.tandfonline.com

Moum 1996, Moum 1996, Etemad-Shahidi and Imberger 2002). Yeates (2007) analyzed a large dataset of directly measured turbulent fluxes in a thermally-stratified lake and found that the net transport, the average of the up- and down-gradient fluxes, was down-gradient and rapidly decreased with increasing Richardson number. This suggests that early models for eddy diffusion parameterization dependent on the Richardson number (e.g. Pacanowski and Philander 1981, Christodoulou 1986, Large *et al.* 1994) may overestimate fluxes. The direct turbulent measurements presented herein show that up-gradient fluxes are ubiquitous even at high shear, resulting in negligible net down-gradient fluxes across a pycnocline. The implication for mixing closures is investigated by incorporating a simple closure for net down-gradient fluxes into a 3D hydrodynamic model.

In such a shallow and highly-stratified estuary, the close proximity between the turbulent bottom boundary layer (TBBL) and the highly-stratified region above it, presents difficulties in modeling turbulent mixing across the water column. In turbulence models, that directly solve a version of the TKE equations (e.g. Li *et al*. 2005, Warner *et al.* 2005), the stratification effect on mixing is usually incorporated by turning off the mixing when the gradient (subscript g) Richardson number $\mathrm{Ri_g}$ exceeds a critical value $\mathrm{Ri_g^c}$, and bounding the mixing length scale l by the Ozmidov scale (Galperin *et al.* 1988). Modelling of continental shelf turbulence shows that this length scale limitation is necessary to force l in the Mellor-Yamada level 2.5 model to follow the buoyancy length scale in the stably-stratified region above the bottom boundary layer (Wijesekera *et al.* 2003). The performance of a shear-based closure and a Richardson number-based closure are herein compared. First, an overview of the field experiment and the background of the Tone River estuary are presented. Then the instrumentation used is described, followed by an analysis of the field data. A comparison between field and model results highlights the difference between the two diffusivity closure schemes. Lastly, the model limitations in terms of diffusivity and grid size dependence are discussed.

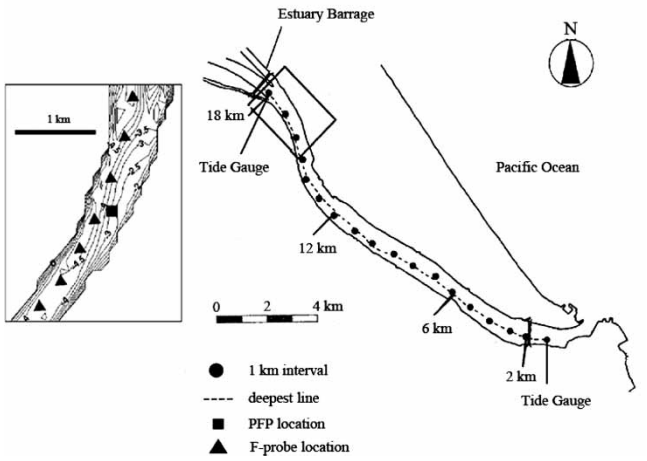

Figure 1 Tone River section showing location of (●) PFP station (▲) and F_probe stations

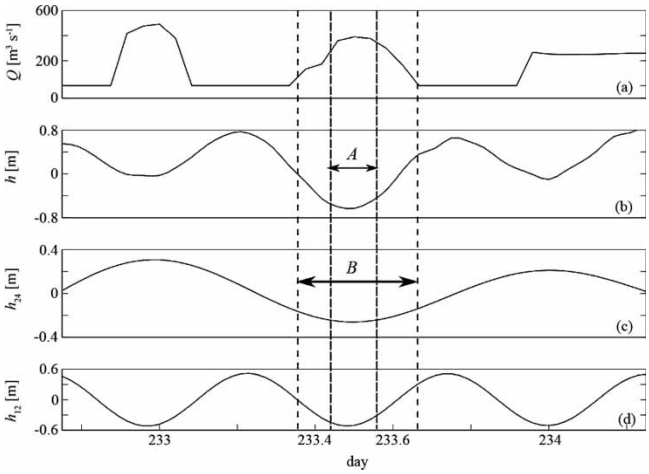

Figure 2 (a) Fresh water discharge from barrage, (b) tidal elevation taken at estuary mouth, (c) semi-diurnal (M2) component, (d) diurnal (M1) tide component. *A* denotes period of PFP data-averaging, *B* period of PFP measurement and ELCOM simulation

2 Field experiment

The experimental tests were conducted in a straight section of estuary 3.5 km long, immediately downstream of the freshwater barrage (Fig. 1). The test was commenced on the 17th and continued through to the 21st of August (days 229 and 233) of 2001 (Fig. 2), during a neap-to-spring tidal transition, providing a large range of both shear and stratification conditions; the discharge was highest on Day 233. The portable flux profiler (PFP) (Imberger and Head 1994) was deployed at a fixed station (Fig. 1), in a free-falling mode (fall velocity from 0.1 to 0.2 m s^{-1}). The PFP was equipped with sensors to measure the microstructure profiles of velocity, salinity and temperature. Velocity was measured with a three-component forward-scatter laser Doppler anemometer, with a measurement resolution of 0.001 m s^{-1} and spatial resolution of about 1 mm horizontal and 3 mm vertical. A combined, high resolution conductivity-temperature sensor (0.0001 S m^{-1}; 0.001 °C) was positioned 2 mm behind the velocity measurement volume providing turbulent flux measurements in a control volume 3 mm long and 2 mm wide. The profiler was also equipped with a compass (resolution 1.4°) and inclinometer (resolution 0.25°) and the sampling rate was 100 Hz.

To understand the evolution of the horizontal gradients of salinity, temperature, pH, DO, turbidity and velocity, longitudinal transects, using a boat-mounted acoustic Doppler current profiler and a fine-scale profiler (Imberger and Head 1994), were performed each 30 min. over the tidal cycle (Fig. 1, inset). The focus here is solely on the microstructure data collected using the PFP under the flow conditions shown in Fig. 2.

3 Data analysis

3.1 *Mean properties from PFP*

The mean properties computed from the PFP data were density, buoyancy frequency, water velocity and shear. The density was obtained from the temperature and conductivity signals that had been sharpened and smoothed using filters to match the different response characteristics of the sensors (Fozdar *et al.* 1985). Both the density and velocity signals were subsequently low-pass filtered at 0.4 Hz, corresponding to a length scale of 25 cm; the buoyancy frequency and shear were then computed at each point in the profile.

As the PFP was a free fall vehicle, the horizontal components of the probe velocity were calculated by integrating the drag force on the probe, as suggested by Hendricks and Rodensbuch (1981) and described by Saggio and Imberger (2001), assuming the PFP came to rest once it had settled on the bottom; the PFP length was around 1 m so that the valid data were obtained only from a depth of about 1.5 m onwards.

3.2 *Turbulent parameters from PFP*

The turbulent components of the velocity and density signals were separated from the mean components with a non-recursive Gaussian filter. To capture the range of the overturn scales that varied greatly over the water column, the filter standard deviation was allowed to vary with the magnitude of the local overturn scale. First, the Thorpe (1977) scale L_T was determined by sorting the density signal into a gravitationally stable profile. Then a centred displacement scale L_C was calculated by displacing L_T by half its magnitudes and averaging the result. The envelope of L_C was then used as the standard deviation of the Gaussian filter. This separation method avoided rippling and phase shifting at the top of the benthic boundary layer (Saggio and Imberger 2001). The next step was to identify segments of the profiles with distinct turbulent properties (Imberger and Ivey 1991). In this segmentation procedure care was taken to identify and minimize the contamination from the signal noise frequency of the instruments, as described by Saggio and Imberger (2001).

Dissipation was estimated by two distinct methods. The first made a direct estimation from the turbulent velocity gradients, by using the axisymmetric assumption (Piccirillo and van Atta 1997).

$$\varepsilon_D = \nu\left(5\overline{\left(\frac{\mathrm{d}w'}{\mathrm{d}z}\right)^2} + \frac{5}{2}\overline{\left(\frac{\mathrm{d}u'}{\mathrm{d}z}\right)^2} + \frac{5}{2}\overline{\left(\frac{\mathrm{d}v'}{\mathrm{d}z}\right)^2}\right) \qquad (1)$$

This was calculated using the auto-spectra of the velocity fluctuations and multiplying by the square of their corresponding wave numbers. The second method involved Batchelor curve-fitting of the temperature gradient signal, using the algorithm of Luketina and Imberger (2001); this dissipation estimate is designated by ε_B. The method minimized the contamination due to internal waves and instrument noise by excluding their corresponding frequency ranges from the spectra prior to curve-fitting. From visual examination of the spectral fit of the bottom segments it was found that ε_B exceeded the algorithm limit of $1 \times 10^{-4}\,\mathrm{m^2\,s^{-3}}$ for many bottom segments. This was probably caused by the bottom segments being too short to contain a long enough record to accurately resolve the roll-off region of the spectrum in the energetic TBBL, resulting in an overestimation of ε_B (Luketina and Imberger 2001). Therefore, ε_B was accepted only from segments for which $|\log(\varepsilon_B/\varepsilon_D)| < 1$.

4 Turbulent closures

4.1 *Vertical diffusivity closures*

Here a basic description of two vertical diffusivity closure schemes used in this study is presented. These are part of an explicit mixing model for the 3D estuary, lake and coastal ocean model (ELCOM) (Hodges *et al.* 2000, Hodges and Imberger 2001, Laval *et al.* 2003, Hodges and Dallimore 2006).

In ELCOM the vertical diffusion term is calculated with an explicit mixing model, based on the integral mixed-layer model of Spigel *et al.* (1986), that is invoked on a per-column basis in the ELCOM 3D fixed-grid framework. In brief, the general mixing model (Hodges *et al.* 2000) mixes vertically adjacent cells whenever the TKE available for mixing is larger than the potential energy required to completely mix the ambient stratification. The mixing loop starts from a surface cell, where the TKE from wind stress is introduced and combined with the TKE available from convection and local internal shear production. If the sum of available energy is larger than that required to mix the adjacent cell below, then mixing proceeds, with the left over energy being used to mix the next lower cell and so on; in this way ,a surface mixed-layer penetrates into the water column via discrete homogenization of the grid cells. Turbulent exchange of scalars and momentum between vertically adjacent cells is quantified in terms of a mixing fraction: the volume-wise percentage of mass/momentum that is exchanged in one time step. Before the diffusivity closure schemes are presented, the relationship between the vertical mass diffusivity, eddy viscosity, and mixing fraction are introduced. Vertical diffusivity of mass may be defined in terms of buoyancy flux and local density gradient as (e.g. Osborn 1980)

$$\kappa_\rho = \frac{\overline{\rho' w'}}{\partial\rho/\partial z} \qquad (2)$$

Interest is in K_ρ, the numerical counterpart of κ_ρ, and its relationship to the mixing fraction. Suppose that a fully mixed-layer of thickness h has exchanged a fraction of its mass F_m with the cell of thickness Δz below. The change in the mean potential energy is then given by

$$\Delta PE = 0.5 F_m g \Delta\rho h \Delta z \qquad (3)$$

where $\Delta\rho$ is the initial density difference between the cells. If it is assumed that the total buoyancy flux may be discretized by $\Delta PE/\Delta t$, then Eqs. (2) and (3) yield

$$K_\rho = \frac{F_m}{2}\frac{h\Delta z}{\Delta t} \tag{4}$$

Under the Boussinesq approximation the change in the mean kinetic energy ΔKE during one time step is

$$\Delta KE = \tilde{\rho}\left(F_m - 0.5F_m^2\right)\Delta U^2\frac{h\Delta z}{(h+\Delta z)} \tag{5}$$

where $\tilde{\rho}$ is the average density after mixing. Therefore, the eddy viscosity may be expressed as

$$K_\upsilon = K_\rho\left(1 - \frac{K_\rho}{h\Delta z/\Delta t}\right) \tag{6}$$

Here two alternative diffusivity closure schemes are presented that differ in how F_m is calculated. The first formulation follows that of Laval *et al.* (2003) (referred to, hereafter, as LIHF), who calculated as $F_m = \Delta T/T_m$, where T_m is the time required to completely homogenize the cells and ΔT is the computation time step assuming a constant shear (Thorpe 1973), so that

$$F_m = \min\left(1, \frac{\Delta T}{T_m}\right) \tag{7}$$

and $T_m = 50|\Delta U/\Delta z_m|^{-1}$, with ΔU as the velocity difference between two vertically adjacent cells and Δz_m as the spacing between the centres of the vertically adjacent cells. Using Eq. (4), the effective diffusivity of the first closure is

$$K_\rho = \frac{h\Delta z}{2\Delta T}\min\left(1, 50\Delta T\left|\frac{\Delta U}{\Delta z_m}\right|\right) \tag{8}$$

The second closure explicitly calculates the net down-gradient diffusivity as a function of the local gradient Richardson number Ri_g. Lake-wide microstructure data from Lake Kinneret (Yeates 2007) indicated that the vertical diffusivity is characterized by two regimes (Fig. 3)

$$\frac{\kappa_\rho}{\kappa_\theta} = 17.6\mathrm{Ri}_g^{-0.54},\ \mathrm{Ri}_g \le 0.0228$$
$$0.04\mathrm{Ri}_g^{-2.11},\ \mathrm{Ri}_g > 0.0228 \tag{9}$$

Yeates (2007) found that this relationship applies for both up- and down-gradient fluxes and the data from the Tone River estuary supported this ascertain (Fig. 3), although the present data are from a more energetic environment with $\mathrm{Ri}_g > 0.0228$; overall, Fig. 3 supports the view that data from a thermally-stratified lake and a salinity-stratified estuary collapse to the same curve with acceptable scatter. Due to the large size of the data set, Yeates (2007) was able to calculate the percentage

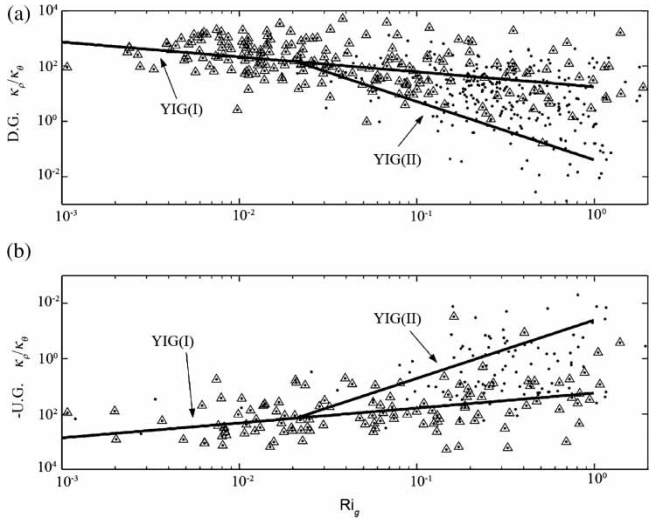

Figure 3 Vertical diffusivity normalized by molecular diffusivity of heat. YIG(I) and YIG(II) represent the curves from Eq. (9) of Yeates (2007). (a) down-gradient, (b) up-gradient fluxes, respectively, with (dots) data from stationary PFP segments taken in Tone River, (triangles) bottom segments

of segments with down-gradient fluxes versus Ri_g. Using least-squares fitting, the resulting relationship was expressed by him as $F_{DG} = -0.406\mathrm{Ri}_g^{-0.102}$. There are not enough segments from the Tone River estuary for high statistical confidence, but the data lend considerable support for this relationship [not shown]. With κ_θ as the molecular diffusivity of heat the resulting net down-gradient diffusivity κ_ρ was thus assumed to be given by (Yeates 2007)

$$\frac{\langle\kappa_\rho\rangle}{\kappa_\theta} \equiv F_{DG}\kappa_\rho = 7.15\mathrm{Ri}_g^{-0.642},\ \mathrm{Ri}_g \le 0.0228$$
$$0.0162\mathrm{Ri}_g^{-2.21},\ \mathrm{Ri}_g > 0.0228 \tag{10}$$

4.2 *Simulation setup*

Simulations were carried out using both closure formulations with two vertical grid sizes of 25 and 12.5 cm, respectively. All simulations used a 100 m × 50 m horizontal grid on a straightened bathymetry (Hodges and Imberger 2001) of Tone River, the downstream forcing being the tidal variation measured 1 km from the mouth of the estuary and the inflow from the barrage as the upstream boundary condition. The focus was confined to day 233, when the freshwater discharge persisted long enough to allow averaging of turbulent field data over a period when the freshwater arrested the salt-wedge. To obtain identical initial conditions for simulations of different vertical grid size, "spin up" simulations were run using a sharpening filter (Laval *et al.* 2003) with various salinity thresholds, matching the salinity and velocity fields to those from the first PFP cast of the day. The computational time step was 25 s, indicating that the upper limit of diffusivity for $\Delta z = 12.5$ cm was four times lower than those for $\Delta z = 25$ cm.

5 Results

The water level, as measured by the tidal gauge 1 km from the river mouth, is shown in Fig. 2 (Fig. 1 for location) together with the discharge from the barrage during the test period. The barrage consisted of nine sluice gates of 465 m total length. The discharge was estimated hourly by measuring the water level up- and downstream of the barrage. In general, the timing of the freshwater release was keyed to the water level difference between the up- and downstream sides of the barrage (Fig. 2). The time of the peak discharge typically coincided with the lowest point of the ebb tide, at which time both the diurnal and the semi-diurnal tidal components were at their lowest amplitude. On day 233 the discharge increased from a low value of 150–400 $m^3\ s^{-1}$ at around 10 am peaking around noon after which time the gates were closed gradually and the inflow ceased at 4 pm.

The staggered profiles of salinity and longitudinal velocity from the two diffusivity closures in ELCOM are shown together with the field data from PFP profiles in Fig. 4 for $\Delta z = 12.5$ cm. No differences were detected between the simulations of mean salinity and velocity with $\Delta z = 12.5$ cm and $\Delta z = 25$ cm so for brevity only the former is shown. To aid comparisons, the PFP data (circles) have been sub-sampled at 25 cm interval and time-interpolated to correspond to the simulation output time-step of 2 min. Evident from the figure is the descent and thickening of the pycnocline with time as the shear increased across the pycnocline from the start to about 15:00 h after which time the salt wedge moved upstream lifting the pycnocline; the simulated data were taken from the grid nearest to the location of the PFP station.

To render a reliable comparison between the computed diffusivity and the direct field measurement, an averaging time window around low tide, between 11 am and 1 pm was chosen, over which time the water level varied less than 20 cm, and the freshwater discharge was at its peak and almost constant; conditions thus represented an approximate steady-state (Fig. 2). Shown in Fig. 5 are the time-averaged field and simulated vertical profiles of the vertical diffusivity. The LIHF closure yielded a diffusivity profile that was almost uniform throughout the water column, and captured only the upper bound of the field diffusivity (the ends of the horizontal lines) in the lower layer, and grossly overestimated the upper layer values; we shall focus, below, only on the results from the YIG (Yeates, Imberger, Gomez forthcoming) closure scheme. By contrast, the YIG closure scheme closely reproduced the values over the whole water column, including the sharp transition between at the top of the benthic boundary layer at a normalized depth of between 0.2 and 0.3. As in the mean field comparison, only the results from $\Delta z = 12.5$ cm simulations for absolute values of diffusivity are presented. The effect of vertical grid resolution was noticeable, but the results qualitatively similar in terms of the profile shape.

The simulation output, for the YIG closure scheme and $\Delta z = 12.5$ cm, are shown in Fig. 6 together with the field results; (a) the shear production of TKE, (b) the dissipation of TKE and (c) the buoyancy flux, all averaged over the same period as the data shown in Fig. 5. The field TKE shear production was high and almost uniform throughout the water column consistent with the large scale shear shown in Fig. 4. In the TBBL, production approximately balanced dissipated (Fig. 6(b)). In the pycnocline region, around a normalized depth of 0.4, the PFP data show that combined dissipation (Fig. 6(b)) and vertical turbulent buoyancy flux (Fig. 6(c)) were slightly larger than the shear production, suggesting that advection of excess TKE was advected into the area. The simulations captured the shear production, dissipation and buoyancy flux reasonably well in the upper half and lower quarter of the water column (Fig. 6(a)), where shear was the largest. However, at the normalized depth of around 0.3, in the region of strongest stratification, the simulated shear production and dissipation were both smaller than the results from the PFP

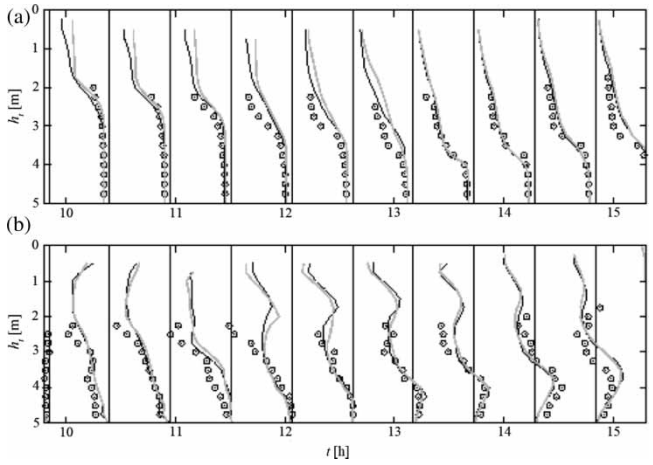

Figure 4 Stagger plot of field and simulated values of (a) salinity (1 h = 30 psu), (b) longitudinal velocity (1 h = 1 ms^{-1}) for $\Delta z = 12.5$ cm. (open circle) field data, (black solid line) ELCOM with YIG closure, (grey solid line) ELCOM with LIHF closure, (dashed grey line) zeros

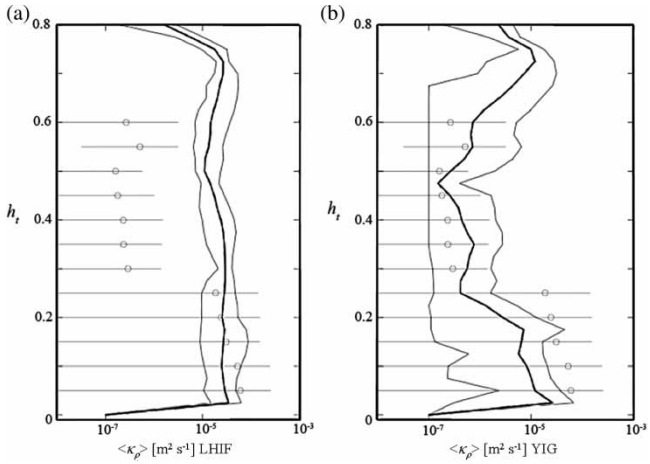

Figure 5 Vertical profiles of turbulent diffusivity time-averaged over 11 am and 1 pm, with (open circle) PFP averages, horizontal (grey dash) distance to maximum and minimum values. Positive floor value was enforced on negative values, with (black solid line) model averages, (black dash) model maximum and minimum for (a) first closure (LIHF), (b) second closure (YIG), $\Delta z = 25$ cm

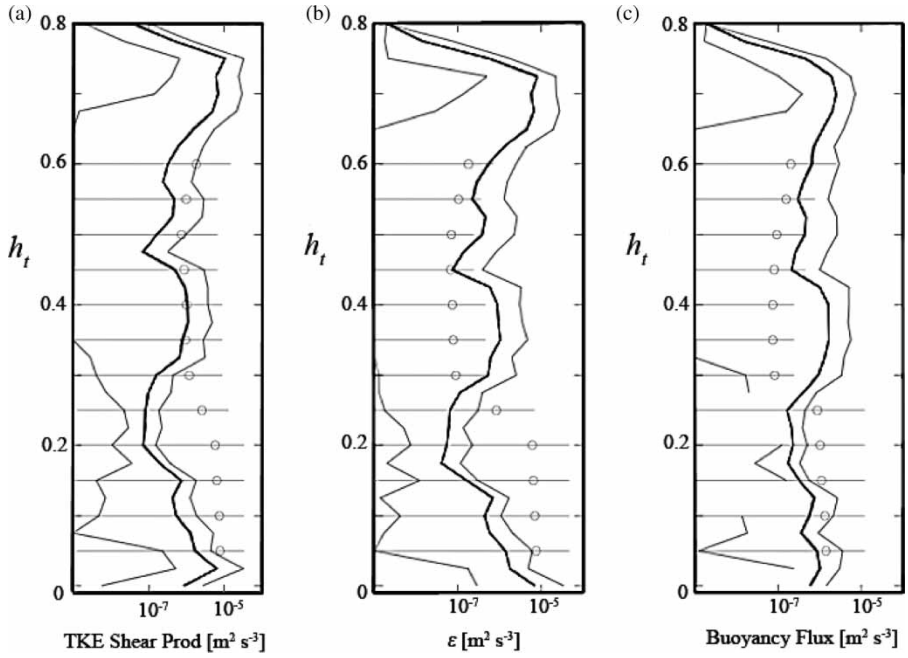

Figure 6 Vertical profiles of (a) TKE production from mean shear, (b) TKE dissipation, (c) buoyancy flux, time-averaged over 11 am and 1 pm, (open circle) PFP averages with error bars. Positive floor value was enforced on negative values. (black line) model averages, (grey line) model maximum and minimum. Only YIG closure was used, $\Delta z = 12.5$ cm

data; higher vertical resolution would be required to match the small overturn scales there.

6 Discussion

As discussed above, the LIHF closure scheme ensures time-step independence (Eq. 7) and the YIG closure scheme ensures both time-step and length-scale independence by implicitly involving a definition of a mixing fraction F_m that includes a mixing length scale L_m, so that

$$F_m = \min\left(1, \frac{L_m^2 \Delta T}{h \Delta z T_m}\right) \tag{11}$$

The microstructure measurements of Saggio and Imberger (2001) suggest that, for stratified, shear-driven turbulence, the Thorpe overturn length scale L_T is proportional to the primitive length scale L_P, where

$$L_T = C\left(\frac{\nu}{N}\right)^{1/2} \tag{12}$$

and $C = 8.3$ from their data (see also Barry *et al.* 2001). By discretizing N as $(-g\rho_o^{-1}\Delta\rho/\Delta z)^{1/2}$, the shear $S = \Delta U/\Delta z$, and assuming that T_m is proportional to S^{-1}, Eqs. (11) and (4) yield

$$\kappa_\rho = 0.5\frac{L_m^2}{T_m} \propto \frac{vC}{\mathrm{Ri}_g^{0.5}} \tag{13}$$

which is of similar form to the first regime of Eq. (9).

On the other hand, a comparison with the LIHF closure scheme, as represented by Eq. (8), suggests that implicit to the LIHF closure scheme is the assumption of a particular ratio of L_m to the vertical grid size, that needs to be obtained by calibration. Hence the interpretation for the diffusivity profiles shown in Fig. 5 is that both closure schemes provide good estimates of the diffusivities in regions of weak stratification regions such as in the TBBL (of normalized height < 0.26) because the mixing length scales are larger than the vertical grid size. It follows that the measured low diffusivity above the TBBL was mainly due to the increased stratification there, limiting the mixing length scale to values below the vertical grid size. In summary, even though the water column contained strong shear, substantial mixing was confined mainly to the bottom and surface layers and the YIG scheme is better able to reproduce this.

The bulk internal Froude number, as defined by Coates *et al.* (2002) for this flow under investigation, was significantly less than 1, implying that the stratification was stronger than the shear and the intense mixing events immediately following the period of maximum freshwater discharge would have been short lived, patchy and contain considerable proportion of collapsing events with up-gradient fluxes; the success of the YIG scheme demonstrated by the results shown in Figs. 4–6, thus shows the validity of the assumption that the average of the up- and down-gradient fluxes, within one computational time step, represent the net down-gradient diffusivity. In other words, it is assumed that one time step is long compared with the overturn time scale. In the simulations discussed above, the overturn time scale is given by L_T/q, where L_T is the Thorpe time scale and q the turbulent velocity scale and typically the PFP data indicate that L_T/q was of order 10s and the computational time step was 25 s, so that:

$$\frac{L_T}{q\Delta t} << 1 \tag{14}$$

7 Conclusions

Time-averaged profiles of turbulent quantities were measured during a period of high shear in the highly-stratified Tone River water column and the results were used to evaluate the suitability of two different vertical diffusivity closure schemes, the first based on a mixing fraction proportional to the ratio of the computational time step to the complete mixing time and the second one on a relationship between the proportionality of up- and down-gradient fluxes as a function of the gradient Richardson number. The two schemes provided the same predictability for those parts of the water column where the stratification was weak and the shear strong, by in regions where the stratification dominated, the gradient Richardson number scheme performed considerably better.

Notation

F_m = mixing fraction (-)
L_T = Thorpe length scale (m)
L_m = mixing length scale (m)
N = Buoyancy frequency (s^{-1})
q = turbulent velocity scale ($m\,s^{-1}$)
Ri = Richardson number (-)
T_m = mixing time scale (s)
$u\prime$, $v\prime$, $w\prime$ = components of turbulent velocity fluctuations ($m\,s^{-1}$)
ΔT = computational time step (s)
ΔU = velocity difference between two vertically adjacent computational cells ($m\,s^{-1}$)
Δz = vertical grid size (m)
$\Delta\rho$ = density difference between two vertically adjacent computational cells ($kg\,m^{-3}$)
κ = diffusivity ($m^2\,s^{-1}$)
ε = TKE dissipation ($m^2\,s^{-3}$)
ν = kinematic viscosity ($m^2\,s^{-1}$)

References

Barry, M.E., Ivey, G.N., Winters, K.B., Imberger, J. (2001). Measurements of diapycnal diffusivities in stratified fluids. *J. Fluid Mech.* 442, 267–291.

Christodoulou, G.C. (1986). Interfacial mixing in stratified flows. *J. Hydraulic Res.* 24(2), 77–92.

Coates, J.M., Guo, Y., Davies, P.A. (2002). Laboratory model studies of flushing of trapped salt water from a blocked tidal estuary. *J. Hydraulic Res.* 39(6), 601–609.

Cudaback, C., Jay, D. (2000). Tidal asymmetry in an estuarine pycnocline: Depth and thickness. *J. Geophys. Res.* 105(C11), 26,237–26,252.

Etemad-Shahidi, A., Imberger, J. (2002). Anatomy of turbulence in a narrow and strongly stratified estuary. *J. Geophys. Res.* 107(C7), 1–7.

Fozdar, F.M., Parker, G., Imberger, J. (1985). Matching temperature and conductivity sensor response characteristics. *J. Phys. Oceanography* 15(11), 1557–1569.

Galperin, B., Kantha, L.H., Hassid, S., Rosati, A. (1988). A quasi-equilibrium turbulent energy model for geophysical flows. *J. Atm. Sci*. 45(1), 55–62.

Gargett, A.E., Moum, J.N. (1996). Mixing efficiencies in turbulent tidal fronts: Results from direct and indirect measurements of density flux. *J. Phys. Oceanography* 25(11), 2583–2608.

Geyer, R., Farmer, D. (1989). Tide-induced variation of the dynamics of a salt wedge estuary. *J. Phys. Oceanography* 19(18), 1060–1072.

Geyer, R., Smith, J. (1987). Shear instability in a highly stratified estuary. *J. Phys. Oceanography* 17(10), 1668–1679.

Grigg, N., Ivey, G. (1997). A laboratory investigation into shear-generated mixing in a salt wedge estuary. *Geophys. Astrophys. Fluid Dynamics* 85(1), 65–95.

Hendricks, P., Rodensbuch, G. (1981). Interpretation of velocity profiles measured by freely sinking probes. *Deep-Sea Res.* 28A, 1199–1213.

Hodges, B., Dallimore, C. (2006). *Estuary, lake and coastal ocean model, version 2, science manual*. Centre for Water Research, University of Western Australia, Perth.

Hodges, B.R., Imberger, J. (2001). Simple curvilinear method for numerical methods of open channels. *J. Hydraulic Eng.* 127(11), 949–958.

Hodges, B.R., Imberger, J., Saggio, A., Winters, K. (2000). Modeling basin-scale internal waves in a stratified lake. *Limnol. Oceanogr.* 45(7), 1603–1620.

Imberger, J., Head, R. (1994). Measurements of turbulent patches in a natural system. *Fundamentals and advances in hydraulic measurements and experimentation*, 1–20, C.A. Pugh, ed. ASCE, New York.

Imberger, J., Ivey, G.N. (1991). On the nature of turbulence in a stratified fluid 2: Application to lakes. *J. Phys. Oceanogr.* 21(5), 659–680.

Ishikawa, T., Suzuki, T., Qian, X. (2004). Hydraulic study of the onset of hypoxia in the Tone River estuary. *J. Env. Eng.* 130(5), 551–561.

Jay, D., Smith, J. (1990). Residual circulation in shallow estuaries 1: Highly stratified, narrow estuaries. *J. Geophys. Res.* 95(C1), 711–731.

Large, W.G., McWilliams, J.C., Doney, S.C. (1994). Oceanic vertical mixing: a review and a model with a nonlocal boundary layer parameterization. *Reviews of Geophysics* 32(4), 363–404.

Laval, B., Imberger, J., Hodges, B., Stocker, R. (2003). Modeling circulation in lakes: Spatial and temporal variations. *Limnol. Ocean.* 48(3), 983–994.

Li, M., Zhong, L., Boicourt, W. (2005). Simulations of Chesapeake Bay estuary: Sensitivity to turbulence mixing parameterizations and comparison with observations. *J. Geophys. Res.* 110, C12004. doi:10.1029/2004JC002585.

Luketina, D.A., Imberger, J. (2001). Determining turbulent kinetic energy dissipation from Batchelor curve fitting. *J. Atmos. Ocean. Tech.* 18(1), 100–113.

Monismith, S., Fong, D. (1996). A simple model of mixing in stratified tidal flows. *J. Geophys. Res.* 101(C12), 28,583–28,595.

Moum, J.N. (1996). Efficiency of mixing in the main thermocline. *J. Geophys. Res.* 101(C5), 12,057–12,070.

Osborn, T.R. (1980). Estimates of the local rate of vertical diffusion from dissipation measurements. *J. Phys. Oceanogr.* 10(1), 83–89.

Pacanowski, R.C., Philander, S.G.H. (1981). Parameterization of vertical mixing in numerical models of tropical oceans. *J. Phys. Oceanogr*. 11(11), 1443–1451.

Pawlak, G., Armi, L. (1997). Hydraulics of two-layer arrested wedge flows. *J. Hydraulic Res.* 35(5), 603–618.

Piccirillo, P., van Atta, C.W. (1997). The evolution of a uniformly sheared thermally stratified turbulent flow. *J. Fluid Mech.* 334, 61–86.

Saggio, A., Imberger, J. (2001). Mixing and turbulent fluxes in the metalimnion of a stratified lake. *Limnol. Oceanogr.* 46(2), 392–409.

Spigel, R.H., Imberger, J., Rayner, K.N. (1986) Modelling the diurnal mixed layer. *Limnol. Oceanogr*. 31(3), 533–556.

Thorpe, S.A. (1973). Turbulence in stably stratified fluids: A review of laboratory experiments. *Boundary-Layer Meteorol*. 5(1–2), 95–119.

Thorpe, S.A. (1977). Turbulence and mixing in a Scottish Loch. *Phil. Trans. R. Soc.* London A 286, 125–181.

Warner, J., Geyer, W., Lerczak, J. (2005). Numerical modeling of an estuary: A comprehensive skill assessment. *J. Geophys. Res.* 110, C05001. doi:10.1029/2004JC002691.

Wijesekera, H.W., Allen, S., Newberger, P.A. (2003). Modeling study of turbulent mixing over the continental shelf: comparison of turbulent closure schemes. *J. Geophys. Res.* 108, C03103. doi 10.1029/2001JC001234.

Yeates, P. (2007). Deep mixing in stratified lakes and reservoirs. *PhD Thesis*. University of Western Australia, Perth.

Yeates, P.S., Gomez-Giraldo, A., Imberger, J. (forthcoming). Relationship between turbulent mixing and the gradient Richardson number in a thermally stratified lake.